



Dynamical proxies of North Atlantic predictability and extremes

Davide Faranda, Gabriele Messori, Pascal Yiou

► To cite this version:

Davide Faranda, Gabriele Messori, Pascal Yiou. Dynamical proxies of North Atlantic predictability and extremes. Scientific Reports, 2017, 10.1038/srep41278 . hal-01340301

HAL Id: hal-01340301

<https://hal.science/hal-01340301>

Submitted on 30 Jun 2016

HAL is a multi-disciplinary open access archive for the deposit and dissemination of scientific research documents, whether they are published or not. The documents may come from teaching and research institutions in France or abroad, or from public or private research centers.

L'archive ouverte pluridisciplinaire **HAL**, est destinée au dépôt et à la diffusion de documents scientifiques de niveau recherche, publiés ou non, émanant des établissements d'enseignement et de recherche français ou étrangers, des laboratoires publics ou privés.

Dynamical proxies of North Atlantic predictability and extremes

Davide Faranda^{1*}, Gabriele Messori² & Pascal Yiou¹

¹Laboratoire des Sciences du Climat et de l'Environnement, LSCE/IPSL, CEA-CNRS-UVSQ, Université Paris-Saclay, F-91191 Gif-sur-Yvette, France

² Met Office Hadley Centre, Exeter, UK

* Correspondence to: Davide Faranda, email: davide.faranda@lsce.ipsl.fr

Main

Atmospheric flows are characterized by chaotic dynamics and recurring large-scale patterns . These two characteristics point to the existence of an atmospheric attractor defined by Lorenz as: “the collection of all states that the system can assume or approach again and again, as opposed to those that it will ultimately avoid”. The average dimension D of the attractor corresponds to the number of degrees of freedom sufficient to describe the atmospheric circulation. However, obtaining reliable estimates of D has proved challenging . Moreover, D does not provide information on transient atmospheric motions, which lead to weather extremes . Using recent developments in dynamical systems theory , we show that such motions can be classified through instantaneous rather than average properties of the attractor. The instantaneous properties are uniquely determined by instantaneous dimension and stability. Their extreme values correspond to specific atmospheric patterns, and match extreme weather occurrences. We further show the existence

of a significant correlation between the time series of instantaneous stability and dimension and the mean spread of sea-level pressure fields in an operational ensemble weather forecast at steps of over two weeks. We believe this method provides an efficient and practical way of evaluating and informing operational weather forecasts.

Dynamical systems analyses led to the crucial notion that atmospheric motions are chaotic and settle on an attractor [1]. Estimates of the average dimensions D of atmospheric attractors were produced from times series of various meteorological variables [2] because this quantity roughly indicates the numbers of degrees of freedom sufficient to describe the flow in its average, time-stationary configuration. However, many weather phenomena of great societal and economic relevance such as extratropical storms, heatwaves and cold-spells are linked to transient metastable states of the atmosphere, whose dynamical properties depend on the instantaneous rather than average properties of the attractor [3]. Such local properties are uniquely determined by two quantities: the local dimension and stability of the state being considered [4].

The concept of instantaneous dimension is intuitive: for a state ζ of the attractor (an atmospheric configuration), the instantaneous dimension $d(\zeta)$ measures the density of neighbouring points (similar configurations). This implies that d can be related to both the entropy and the predictability of nearby trajectories [5]. The stability of the state ζ is measured by the stickiness $\theta(\zeta)$ defined as the inverse of the average persistence time of trajectories around ζ . If ζ is a fixed point of the dynamics, $\theta(\zeta) = 0$. For a point that leaves the neighbourhood of ζ immediately, $\theta = 1$. In general, the stickier the point ζ , the longer the previous and subsequent states of the system will resemble ζ .

These instantaneous properties have not been previously computed for atmospheric flows for two main reasons: i) until recently the length of high-frequency, geographically extensive me-

teorological time series has been insufficient to allow reliable estimates ii) the methodologies used to compute the average dimension of the attractor were not suited to the purpose. In this paper we compute the distribution in phase space of the instantaneous dimensions $0 < d < \infty$ and the stickiness $0 < \theta < 1$ for daily sea-level pressure (SLP) fields in the North Atlantic, by applying a novel methodology based on the universal behavior of the Poincaré recurrences in chaotic systems [4]. This methodology is general, and thus applicable to a wide range of dynamical systems beyond climate science. There are two key advances relative to previous attempts: first, our methodology removes major uncertainties associated with past estimates [6, 2] (see Methods). Second, it yields the full probability distribution of the instantaneous dimension of the attractor. The validity of our approach has been successfully tested on the idealized Lorenz system [7] and on a number of synthetic fields (Extended Data Figs A.1 and A.2).

We chose SLP as a representative field for the large-scale atmospheric circulation over the North Atlantic and Europe (see Methods). To verify the robustness of our results we analysed two distinct daily SLP timeseries: the NCEP/NCAR [8] and ERA-Interim data [9]. The average dimensions D obtained by averaging d over all ζ , including tests performed on coarse-grained NCEP/NCAR data, are shown in Fig. 1-a. If we interpret the resolution, which is of order 10^4 grid-points for ERA-Interim and of order 10^3 grid-points for NCEP/NCAR, as an upper bound for D , our results point to the existence of a low dimensional attractor. The values of D are comparable across all resolutions, except when the coarse graining degrades the resolution to the point where large-scale SLP low and high centers become unrecognizable (resolution 20°) and the phase space itself is shrinking. We find that the distribution of $d(\zeta)$ for the 2.5° NCEP/NCAR reanalysis ranges from as low as 3 to as high as 20 (Fig. 1-b). The average value $D = 13$ is only representative of a limited number of daily pressure fields.

Our estimate of D is not the dimension of the global climate attractor: here we focus on a

specific region and we analyse SLP structures with a well defined radius. The large spread in the distribution of instantaneous dimensions ($3 < d(\zeta) < 20$) explains why deterministic low dimensional models are unable to reproduce the transients between metastable states of the atmospheric circulation, such as the transitions between zonal and blocked phases of the mid-latitude flow [1, 3].

Figure 1-c displays the time series of $d(\zeta)$. A seasonal cycle is identifiable both from the whole time series and from the inset which shows the last three years of instantaneous dimension estimates. The troughs occur in summer and the peaks in winter, when the temporal variability of the instantaneous dimension is also high. The corresponding results for ERA-Interim are shown in Extended Data Fig. A.3.

We now use $d(\zeta)$ and $\theta(\zeta)$ as probes to investigate the large-scale dynamics and associated weather extremes of the North Atlantic. Here we only discuss the results for the highest resolution NCEP/NCAR data (see Extended Data Figs. A.4 and A.5 for the ERA-Interim results). The analysis of idealised systems, such as the one proposed by Lorenz[7], suggests that extremes in d and θ trace extremes in phase space (see Extended Data Fig. A.1 and Methods). We begin by isolating all the days t such that the instantaneous dimension d and persistence θ are beyond the 0.02 and 0.98 quantiles of the respective distributions. The results are insensitive to the exact choice of quantile. The North Atlantic SLP experiences a strong seasonal cycle with significant changes in the principal atmospheric patterns and modes of variability between the winter and summer seasons (e.g. ref. [10]). If extremes in the instantaneous properties have a direct correspondence to the large-scale circulation, a similarly pronounced seasonal cycle in their occurrence might be expected. Indeed, the dimensional extremes occur almost exclusively during the extended boreal winter period, as do the maxima of θ (Fig. 2). The θ minima, on the opposite, occur from early summer into winter. Since these are the most persistent patterns, the summertime episodes might be linked to the more staid character of the stable dynamics during

89 this season. Fig. 3 displays the pairs (θ, d) for each day.

90 The SLP anomaly patterns corresponding to the extremes in the instantaneous dimension $d(\zeta)$
91 and persistence $\theta(\zeta)$ are shown in the four side panels of Fig. 3. As expected, they correspond to
92 very large SLP anomalies. More surprisingly, all four composites resemble well-known large-
93 scale weather regimes [11, 12, 13]. The persistence of the patterns ranges between three days
94 and just over one day ($0.3 < \theta < 0.8$). This should not be compared directly to the persistence
95 of the traditional weather regimes, as the requirement that the flow does not leave the neighbour-
96 hood of the state ζ is a more restrictive condition than that imposed by clustering algorithms.
97 The minima in daily dimension correspond to positive North Atlantic oscillation (NAO) condi-
98 tions, which favour the occurrence of cyclones across the North Atlantic [14], and destructive
99 surface winds over continental Europe [15]. Indeed, we find a statistically significant match
100 between these low instantaneous dimensions and historical storms: the names and dates of storms
101 corresponding to minima of $d(\zeta)$ are reported in Fig. 4 (see also methods). Conversely, minima
102 of $\theta(\zeta)$ match the NAO- regime. Both NAO phases have a strong impact on the downstream
103 temperature extremes over Europe [16]. However, we note that there are differences between
104 the impacts of the traditional weather regimes and the patterns we identify here (see Extended
105 Data Fig. A.6 and Methods). From the dynamical systems perspective, the negative NAO has
106 a systematically longer persistence than the positive phase. Both the largest and the smallest
107 NAO values mostly display below-average $d(\zeta)$, thus affording good predictability in accor-
108 dance with recent analyses of ensemble prediction systems [17]. The maxima of $\theta(\zeta)$ and $d(\zeta)$
109 are both associated with a blocked zonal flow and resemble the Atlantic Ridge and the Block-
110 ing regimes, respectively. These are linked to European temperature extremes, although our
111 patterns again display some novel connections (see Extended Data Fig. A.7 and Methods).
112 Blocked zonal flows are notoriously difficult to forecast [17]. This is due to the transition from
113 persistent low instantaneous dimensions to less persistent, higher dimensions as the atmosphere

shifts from a zonal NAO-type flow to a blocked configuration.

We argue that these results can be used in an operational forecast system. If our dynamical indicators are indeed linked to predictability, given a certain state they should correlate with the skill of the model in predicting the future states of the field. We test this by correlating the values of d and θ for the period 2000-2015 with the output of the 2nd Generation NOAA Global Ensemble Reforecast (GER) data set [18]. This is consistent with the current operational NCEP Global Ensemble Forecast System (GEFS), and consists of 11 ensemble members. The ensemble spread at different forecast hours is defined as: $\langle\sigma_{SLP}\rangle$, where angular brackets indicate spatial averages over the region considered in the analysis.. The correlation coefficient R is significant at all forecast steps at the 0.05 significance level, reaching $R(\theta, \langle\sigma_{SLP}\rangle) = 0.42$ and $R(d, \langle\sigma_{SLP}\rangle) = 0.2$ (see Extended Data Fig. A.10-a for the complete analysis). While these values are not high for forecasts a short time ahead, their persistence at steps of over two weeks is noteworthy. Figure 5a), b) shows the bivariate histograms of $(d, \langle\sigma_{SLP}\rangle)$ and $(\theta, \langle\sigma_{SLP}\rangle)$ for the forecast step of 384 hours ahead initialized on all days in the data set. There is a strong linear relationship between θ and $\langle\sigma_{SLP}\rangle$, although the histogram suggests that the distribution is not uniform and peaks at either at low ($\langle\sigma_{SLP}\rangle \simeq 400$ Pa) or high ($\langle\sigma_{SLP}\rangle \simeq 800$ Pa) values. This latter feature might be dependent on the reforecast product. The analysis further suggests that θ is a better proxy of ensemble spread $\langle\sigma_{SLP}\rangle$ than d . The ensemble spread is a generic measure of the dispersion of the trajectories whereas d and θ provide different but complementary information on how the trajectories spread. d is linked to the entropy and therefore to the maximum divergence of the trajectories whereas θ indicates how the trajectories stick together. A high stability implies that only few members strongly deviate from the bulk so that $\langle\sigma_{SLP}\rangle$ is linked to θ (in most of the cases). On the rarer cases when most members strongly deviate from each other, we observe a positive correlation between $\langle\sigma_{SLP}\rangle$ and d and a weakened link with θ . For illustration, we report two examples of both situations in Fig. 5-c (low spread in the

ensemble reforecast), and Figure 5-d (high spread in the ensemble reforecast).
The daily dimension and persistence therefore have an immediate practical use as proxies for predictability, and could be fruitfully used as a time-effective way in which to evaluate and inform operational forecast systems. For example, one could imagine a system which determines the resolution and ensemble size for a given initialization step based on the values of d and θ . Moreover, the visualization of the trajectory for a given season (see the supplementary video) can be used to provide a day-by-day tracking of weather extreme events.

Acknowledgments

D. Faranda and P. Yiou were supported by ERC grant No. 338965-A2C2. DF acknowledges V Lucarini, B Dubrulle, F Daviaud, A Jezequel, MC Alvarez-Castro and for useful discussions. ECMWF data were accessed at <http://apps.ecmwf.int/datasets/>. NCEP/NCAR data was obtained at: <http://www.esrl.noaa.gov/psd/data/reanalysis/reanalysis.shtml>.

Author contributions

DF conceived and designed the study. DF and GM performed the dynamical systems analysis, and interpreted the results. DF further tested the technique on idealized systems and compiled the storms database. GM performed the analysis on extreme weather. All authors contributed to the interpretation of the results and the editing of the manuscript.

References and Notes

- [1] Lorenz, E. N. Attractor sets and quasi-geostrophic equilibrium . *J. Atmos. Sci.* **37**, 1685–1699 (1980).

- [2] Grassberger, P. Do climatic attractors exist? . *Nature* **323**, 609–612 (1986).
- [3] Vautard, R. & Ghil, M. Singular spectrum analysis in nonlinear dynamics, with applications to paleoclimatic time series . *Physica D* **35**, 395–424 (1989).
- [4] Lucarini, V. *et al.* *Extremes and Recurrence in Dynamical Systems*. Pure and Applied Mathematics: A Wiley Series of Texts, Monographs and Tracts (Wiley, 2016). URL <https://books.google.fr/books?id=ebTOoQEACAAJ>.
- [5] Young, L.-S. Dimension, entropy and Lyapunov exponents . *Ergod. Theor. Dyn. Syst.* **2**, 109–124 (1982).
- [6] Takens, F. *Detecting strange attractors in turbulence* (Springer, 1981).
- [7] Lorenz, E. N. Deterministic nonperiodic flow . *J. Atmos. Sci.* **20**, 130–141 (1963).
- [8] Kalnay, E. *et al.* The NCEP/NCAR 40-year reanalysis project . *Bull. Am. Meteorol. Soc.* **77**, 437–471 (1996).
- [9] Dee, D. *et al.* The ERA-Interim reanalysis: Configuration and performance of the data assimilation system . *Quart. J. Roy. Meteor. Soc.* **137**, 553–597 (2011).
- [10] Folland, C. K. *et al.* The summer North Atlantic Oscillation: past, present, and future . *J. Clim.* **22**, 1082–1103 (2009).
- [11] Hurrell, J. W. Decadal trends in the North Atlantic Oscillation: regional temperatures and precipitation . *Science* **269**, 676–679 (1995).
- [12] Yiou, P. & Nogaj, M. Extreme climatic events and weather regimes over the North Atlantic: When and where? . *Geophys. Res. Lett.* **31(7)** (2004).

- [13] Moore, G., Renfrew, I. A. & Pickart, R. S. Multidecadal mobility of the North Atlantic oscillation . *J. Clim.* **26**, 2453–2466 (2013).
- [14] Gómara, I., Rodríguez-Fonseca, B., Zurita-Gotor, P. & Pinto, J. G. On the relation between explosive cyclones affecting Europe and the North Atlantic Oscillation . *Geophys. Res. Lett.* **41**, 2182–2190 (2014).
- [15] Messori, G. & Caballero, R. On double Rossby wave breaking in the North Atlantic . *J. Geophys. Res.* **120(21)** (2015).
- [16] Rogers, J. C. North Atlantic storm track variability and its association to the North Atlantic Oscillation and climate variability of northern Europe . *J. Clim* **10**, 1635–1647 (1997).
- [17] Ferranti, L., Corti, S. & Janousek, M. Flow-dependent verification of the ECMWF ensemble over the Euro-Atlantic sector . *Quart. J. Roy. Meteor. Soc.* **141**, 916–924 (2015).
- [18] Hamill, T. M. *et al.* NOAA’s second-generation global medium-range ensemble reforecast dataset . *Bull. Am. Meteorol. Soc.* **94**, 1553–1565 (2013).
- [19] Grassberger, P. & Procaccia, I. Dimensions and entropies of strange attractors from a fluctuating dynamics approach . *Physica D* **13**, 34–54 (1984).
- [20] Halsey, T. C., Jensen, M. H., Kadanoff, L. P., Procaccia, I. & Shraiman, B. I. Fractal measures and their singularities: the characterization of strange sets . *Phys. Rev. A* **33**, 1141 (1986).
- [21] Lorenz, E. N. Dimension of weather and climate attractors . *Nature* **353**, 241–244 (1991).
- [22] Freitas, A. C. M., Freitas, J. M. & Todd, M. Hitting time statistics and extreme value theory . *Probab. Theory Rel.* **147**, 675–710 (2010).

- [23] Lucarini, V., Faranda, D. & Wouters, J. Universal behaviour of extreme value statistics for selected observables of dynamical systems . *J. Stat. Phys.* **147**, 63–73 (2012).
- [24] Pickands III, J. Statistical inference using extreme order statistics . *Ann. Stat.* 119–131 (1975).
- [25] Grassberger, P. & Procaccia, I. Characterization of strange attractors . *Phys. Rev. Lett.* **50**, 346 (1983).
- [26] Comas-Bru, L. & McDermott, F. Impacts of the EA and SCA patterns on the European twentieth century NAO–winter climate relationship . *Quart. J. Roy. Meteor. Soc.* **140**, 354–363 (2014).
- [27] Cassou, C. Intraseasonal interaction between the Madden–Julian oscillation and the North Atlantic oscillation . *Nature* **455**, 523–527 (2008).

Methods

Attractors are geometrical sets which hosts all the trajectories of a system. To characterize an attractor, one wants to know how often the state ζ occurs over a certain time interval and how long the dynamics stick to ζ before leaving its neighbourhood. If one is able to specify such properties for all the points of the attractor, then the behaviour of the system is entirely known. The general problem one faces in reconstructing an attractor is the limited number of trajectories that can be observed or simulated [2]. In the case of climate observations we have just one single trajectory $x(t)$ (here represented by the time series of SLP daily fields) that we can exploit to reconstruct the attractor properties.

The purpose of our methodology it is to use just a long trajectory $x(t)$ of systems states to reconstruct the salient properties of the attractor. The method is based on the link between

extreme value theory (where the extremes are the recurrences of the points ζ with respect to all the possible states of the system) and the Poincaré theorem of recurrence. The idea is that each state of the system $x(t)$ approximates a point ζ on the attractor and its neighbours are all the states whose distance with respect to $x(t)$ is small. So at each time t and for each state x observed we can define instantaneous properties: the instantaneous dimension d and the stickiness θ . For the theoretical details, demonstrations and examples on dynamical systems see [4]. These properties are instantaneous because they change at each instant t , but they are also local, because states observed at different times but close in the phase space will have similar instantaneous properties. We refer to instantaneous dimensions rather than to local dimension to avoid ambiguity with the notion of local to indicate a geographic region.

Instantaneous Dimensions

The distribution of instantaneous dimension of the attractor of a dynamical system gives useful information on the predictability of observed states because it is related to the Lyapunov exponents [5]. Therefore, estimating the dimension distribution in phase space helps characterizing the overall dynamics of the system. The embedding methods developed in the 1980's [19, 20] do not provide instantaneous dimensions but only the average dimension of the attractor. Moreover, such computations have proved to be problematic in systems with large numbers of degrees of freedom and have given controversial results when applied to atmospheric flows [2, 21].

The method we adopt in the present study results from the application of extreme value theory to the field of dynamical systems [22, 4]. In this approach, the points on the attractor are fully characterized by parameters of extreme value laws: if one fixes an arbitrary point ζ on a chaotic attractor and consider the probability P that a trajectory $x(t)$ returns within a sphere of radius ϵ centered on the point ζ , then the Freitas-Freitas-Todd theorem [22] modified in [23] states

247 that such probability is a generalized Pareto distribution [24]. The time series of the distance
 248 between ζ and the other observations along the trajectory is defined by:

$$g(x(t)) = -\log(\delta(x(t), \zeta))$$

249 $\delta(x, y)$ is a distance function between two vectors, which tends to zero when x and y are close to
 250 each other. Taking the logarithm increases the discrimination of small values of $\delta(x, y)$ which,
 251 as described below, correspond to large values of $g(x(t))$. The probability of logarithmic returns
 252 can then be expressed as:

$$P(g(x(t)) > q, \zeta) \simeq \exp \left[-\frac{q - \mu(\zeta)}{\sigma(\zeta)} \right]$$

253 namely an exponential law whose parameters μ and σ depend on the point ζ chosen on the
 254 attractor. Remarkably, $\sigma(\zeta) = 1/d(\zeta)$, where $d(\zeta)$ is the dimension around the point ζ . This
 255 result has been proved theoretically and verified numerically in several studies collected in [4].
 256 In the above equation, q is a high threshold, and is linked to the radius ϵ via $q = g^{-1}(\epsilon) =$
 257 $\exp(-\epsilon)$. In other words, requiring that the trajectory falls within a sphere around the point ζ is
 258 equivalent to asking that the series of $g(x(t))$ is over the threshold q , which can be simply set
 259 as a percentile of the series itself. If this approach is iterated for several different ζ points, the
 260 attractor dimension is then obtained as:

$$D = \overline{d(\zeta)}$$

261 where the overbar means averaging over all ζ . This is a powerful result because it provides a
 262 direct way to compute dimensions on the attractor without the need for embedding.

Stickiness (persistence) in phase space

The previous results hold when the state ζ considered is not in the vicinity of a fixed point of the attractor. Fixed points are such that $x(t+1) = x(t)$, for all t , i.e. the system is stuck in the same state for an infinite time. In most natural systems, fixed points are unstable: a trajectory passing close to a fixed point spends a finite amount of time in its vicinity before leaving. Such time can also be computed by introducing a further parameter in the previous law. This parameter, known as extremal index, is indicated with θ and is such that:

$$P(g(x(t)) > q \simeq \exp \left[-\theta \left(\frac{x - \mu(\zeta)}{\sigma(\zeta)} \right) \right]$$

We can interpret θ as a measure of the residence time of consecutive iterations in the small sphere around the point ζ . In this interpretation, the inverse of θ is precisely the mean residence time within the sphere.

Some idealized examples

We illustrate the procedure to compute the instantaneous dimension described above by applying it to the Lorenz system [7]. This system and its attractor (often referred to as the Lorenz butterfly) has been studied extensively in the literature, and therefore allows us to compare the results of our approach to those of standard techniques in dynamical systems analysis. We begin by generating a trajectory $\vec{x}(t)$, using a time step of 0.025. Next, we select approximately 75,000 locations along the trajectory as our ζ points on the attractor.

For each ζ : i) the series $g(\vec{x}(t), \zeta)$ is computed, ii) a high threshold q is selected (here the 98th percentile of the series g), iii) a Generalized Pareto distribution is fitted to the observations exceeding the threshold q , iv) an instantaneous dimension of the attractor $d(\zeta)$ is then obtained. Extended Data Fig. A.1) displays the values of the instantaneous dimension at all points along our trajectory, while panel (b) displays the corresponding histogram. It is interesting to observe

that the minima and maxima of the instantaneous dimension track the extremes of the Lorenz [7] attractor. Maxima of the dimension have a non-trivial structure and are found where recurrences are rare — namely in the wings of the butterfly — and where the trajectories diverge the most — namely between the two wings. The minima correspond to the centre of the butterfly wings, i.e. the fixed points of the Lorenz 63 system. The average value of all the $d(\zeta)$ is, by definition, the attractor dimension D . The value we find: $D = 2.06$, corresponds exactly to the value proposed by Grassberger and Procaccia [25]. For this specific example, any q larger than the 95th quantile of g yields the same results. The stickiness, measured in terms of θ is instead shown in Extended Data Fig. A.1). The Lorenz attractor consists of three unstable fixed points: two at the center of the wings and one at the origin of the axes. The three points are well captured by the statistics of θ .

The embedding methodologies adopted in the 1980s were unable to estimate high attractor dimensions [2], thus providing artificially low values for complex systems. To verify that our methodology does not suffer from the same bias, we have applied it to test fields of the same grid-size as the NCEP data set. For completely random fields, we have obtained estimates for D larger than 80. Conversely, estimates of D for fields with coherent structures resembling pressure centres were lower than 5 (see Extended Data Fig. A.2).

Sea-level pressure data

In this study we adopt sea-level pressure (SLP) as the meteorological variable to describe the North Atlantic circulation. The major modes of variability affecting the North Atlantic are often defined in terms of the empirical orthogonal functions of SLP [13, 11], and a wealth of other atmospheric features, ranging from teleconnection patterns to storm track activity to atmospheric blocking can be diagnosed from the SLP field [26, 16].

We base our study on NCEP/NCAR reanalysis data [8] over the period 1948-2015, with a hori-

zontal resolution of 2.5° and ERA-Interim data [9] over 1979-2011 with horizontal resolutions of 0.75° and 1.5° respectively. We consider a domain spanning the North Atlantic and Europe ($80^\circ \text{ W} \leq \text{Long.} \leq 50^\circ \text{ E}$, $22.5^\circ \text{ N} \leq \text{Lat.} \leq 70^\circ \text{ N}$). Further tests show that the results are linearly insensitive to the exact boundaries chosen (Extended Data Fig. A.8).

For the NAO, we use daily values computed by NCEP's Climate Prediction Center. The values are based on NAO patterns which vary on a monthly basis, and cover the full year. The data is freely available from: <http://www.cpc.ncep.noaa.gov/products/precip/CWlink/pna/nao.shtml>

Statistical significance and robustness of the results

For general problems where the value of D is not known a priori, the appropriateness of the value of q for a given ζ can be tested using a number of statistical approaches. In the present study we use the Anderson-Darling test [28] to reject the hypothesis that all $g(x(\vec{t}), \zeta) > q$ come from a generalized Pareto distribution. The test can be repeated for each ζ to obtain a statistical confidence level for the chosen q . All the results displayed in the paper use $q = 0.98$, which satisfies the Anderson-Darling test at the 0.05 confidence level for more than 95% of the chosen ζ . We further performed a visual inspection of the results, and found them to be stable for $0.99 \geq q \geq 0.975$. In fact, if a too high threshold is selected, the number of values exceeding it is insufficient to successfully fit the generalized Pareto distribution.

The results presented in Fig. 2 and 3 in the main text for the NCEP/NCAR data have been repeated for the ERA-Interim reanalysis, and are shown in Extended Data Figs. A.4 and A.5 for both the 0.75° and 1.5° resolutions. It can be seen that both the histograms and the seasonal variability of the instantaneous dimensions are very similar across the three data sets.

Storm database

We present a database of historical storms (see Supplementary Information) which affected Europe between 1948 and 2015. This database is largely based on the Lamb [29] and the Roberts et al. [30] catalogues. Additional storms have been integrated because of their relevance in terms of human losses, damages or their profile in the media. This results in a total of 336 storms. The database is organized in four columns: 1) the day of occurrence in the format `yyyymmdd`, 2) the name(s) of the storm, 3) the countries or the region affected and 4) a reference to a peer-reviewed article, a report or a press article describing the importance of the storm. As a caveat to our methodology, we note that the increasing coverage of both meteorological instruments and technological means of information results in an increasing number of storms with time (whereas the minima of the instantaneous dimensions are equally distributed over time).

We use the database to evaluate the correspondence between the minima of the instantaneous dimensions, which equates to positive NAO-like SLP anomalies, and storminess. A day is said to match a storm if it falls within 2 days of the date specified in the database. Among the 481 minima (corresponding to the quantile 0.02) identified in the NCEP/NCAR data, 17% (namely 82 days) match historical storms recorded in our database. This is a very high percentage: if an equal number of random days is selected (from the extended winter period over which the dimensional extremes occur), statistically only 2.5% will match a historical storm. Examples of well-known storms matching dimensional extremes include Dirk and Herta (see Fig. 4).

Temperature and precipitation extremes

Weather regimes can explain a large part of the statistical distribution for surface variables, and have been linked to anomalies in the frequencies of extreme weather events [12]. Here we show that the extremes in phase space we discuss in the main text have a direct link to the occurrence

of extreme weather events. At the same time, we note that there are some differences relative to previous analyses based on the traditional weather regimes. Extreme events are defined by the 0.98 quantile of the distribution of the anomalies for each gridbox and variable during an extended winter season (September-April). The latter matches the period of occurrence of the vast majority of the phase space extremes. A value of 1 means that the selected days are not discriminating for extremes, while 0 means that there is no chance of an extreme occurring on those days. A value of 2 indicates that the extreme is twice as likely to occur relative to the wintertime climatology. Similarly, a value of 0.5 corresponds to a halved frequency. Statistical significance is evaluated at the 5% level using a montecarlo method. This is indicated in the figures by the grey shading.

Extended Data Fig. A.6 displays the relative changes in the frequency of extreme cold events for (a) high and (b) low $d(\zeta)$. High dimensions show enhanced cold spell frequencies over Scandinavia and northern Europe and the Mediterranean basin. The large signal over Scandinavia is not typically associated with blocking [12], and is possibly linked to the more eastern location of the high in our pattern. The low dimensions shows very large increases in cold extremes over the western North Atlantic and Greenland and south-eastern Europe, matching closely the temperature anomaly footprint of the positive NAO. The link with rainfall extremes (Extended Data Fig. A.6-c,d) is less clear. For the high dimensions, significant changes in Europe are limited to regional decreases in extreme wet days over the British Isles and Scandinavia. The low dimensions display instead regional increases over Scandinavia and continental Europe.

Extended Data Fig. A.7 displays the relative changes in the frequency of extreme cold events for (a) high and (b) low θ . High θ events correspond to frequency increases over the Mediterranean region, in agreement with a similar analysis by Cassou [27]. The low θ match instead a strongly enhanced likelihood of cold extremes over the British Isles and Scandinavia, similarly to the impact of the negative NAO phase. Extended Data Figs. A.7 c, d displays the results for wet

extremes, which again display less significant links. The most robust feature over Europe is a decrease in the frequency of extreme wet days over the British Isles and Northern France for low θ values. In contrast, previous analyses have highlighted the role of a positive NAO in driving wet extremes over these areas[12, 27] .

Methods References

- [29] Anderson, T. W. & Darling, D. A. Asymptotic theory of certain goodness of fit criteria based on stochastic processes. *Ann. Math. Stat.* 193–212 (1952).
- [30] Lamb, H. & Frydendahl, K. Historic Storms of the North Sea, British Isles and Northwest Europe (Cambridge University Press, 1991).
- [31] Roberts, J. et al. The XWS open access catalogue of extreme European windstorms from 1979 to 2012 . *Nat. Hazards and Earth Syst. Sci.* **14**, 2487–2501 (2014).

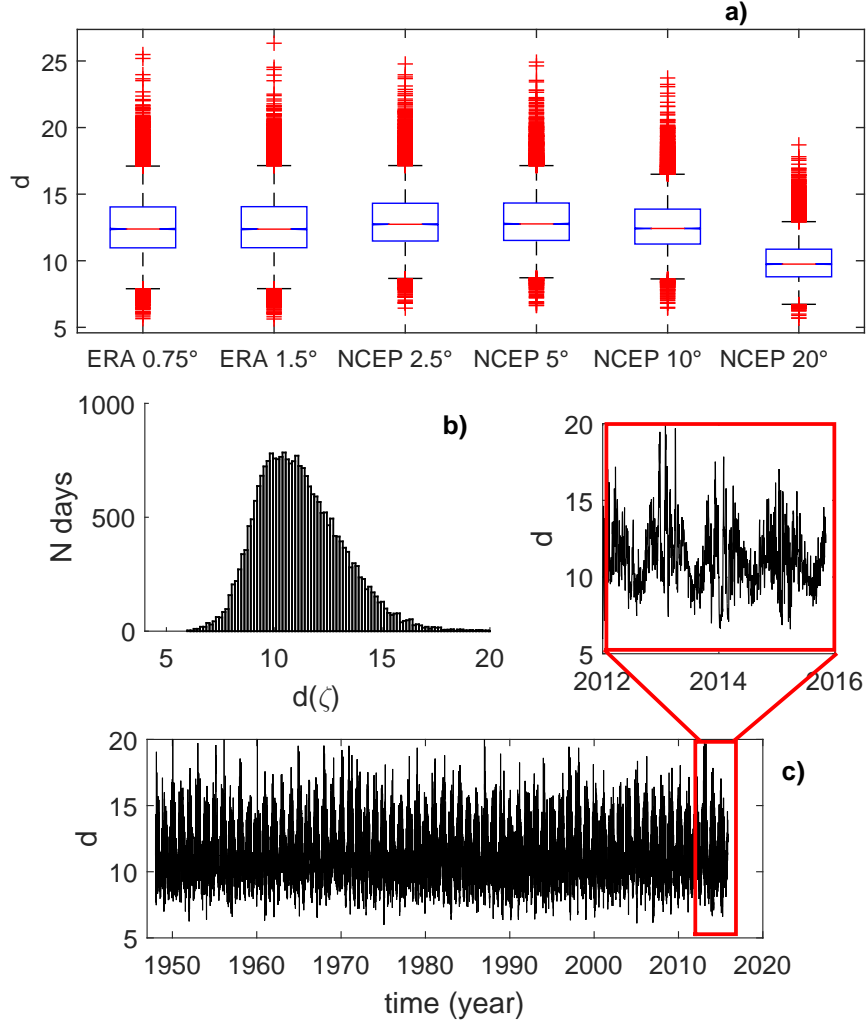


Figure 1: **Analysis of the distribution of instantaneous dimensions.** a) Box-plots of the distribution of $d(\zeta)$ for different resolutions (in degrees of longitude and latitude). In each box, the central mark is the median, the edges of the box are the 25th and 75th percentiles, the whiskers extend to the most extreme data points not considered outliers and outliers are plotted individually. b) Histogram of the daily dimension $d(\zeta)$ for the NCEP reanalysis. c) Time series of the instantaneous dimensions and inset showing the last 3 years.

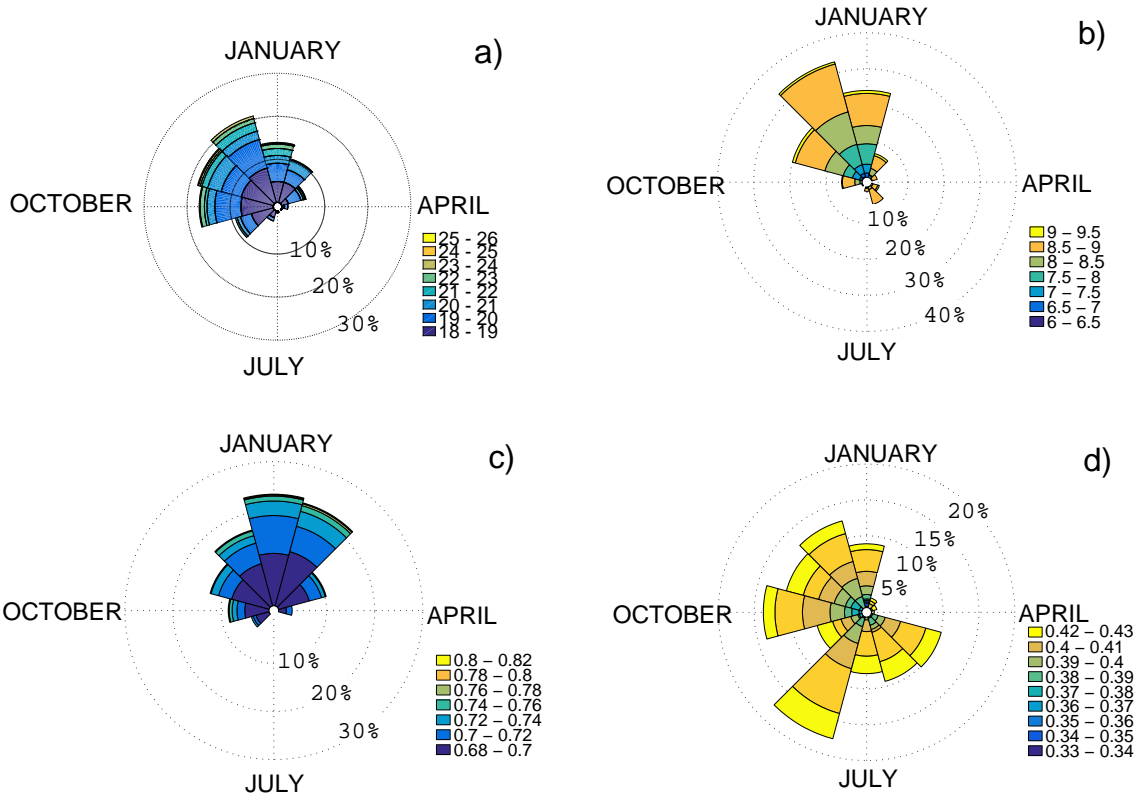


Figure 2: **Monthly distribution of the instantaneous properties exceeding the 0.02 and 0.98 quantiles of their respective distributions.** Maxima of a) d and (b) θ and minima of (c) d and θ (d) for the NCEP reanalysis. The percentage values indicate the occurrences in each month. The colourscale refers to the values of the quantities.

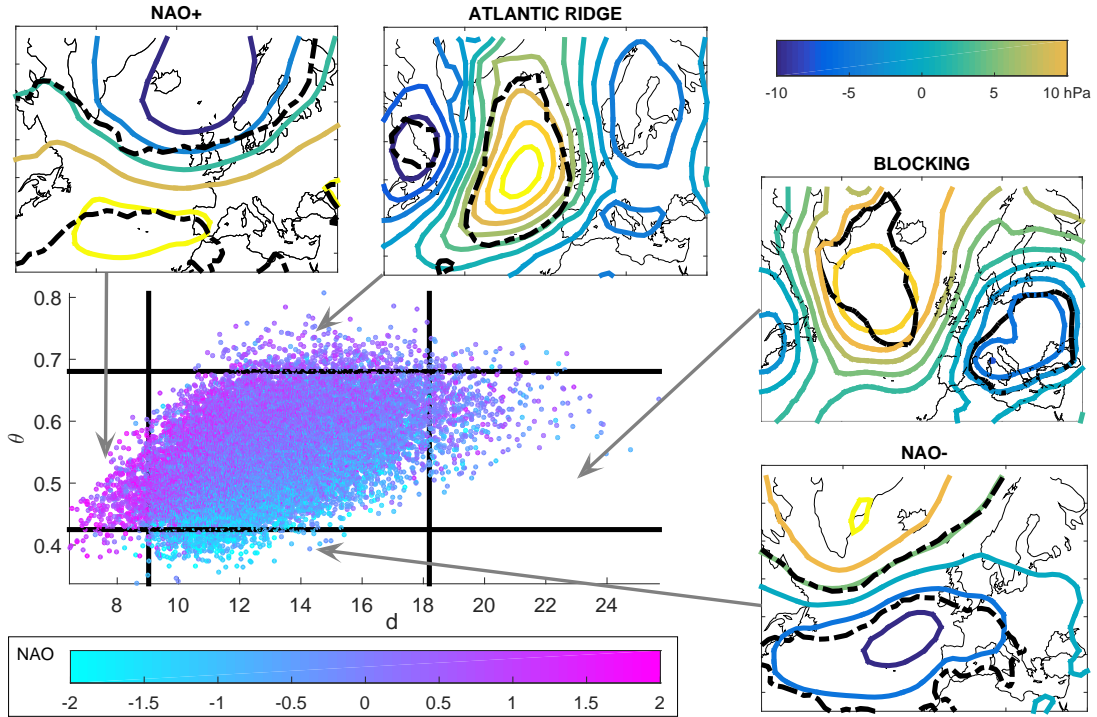


Figure 3: **Dynamical systems analysis for the NCEP reanalysis.** The scatter plot displays the daily values of the instantaneous dimension d and the persistence θ of the field. The NAO value for that day is indicated by the colourscale (increment of four years). The black solid lines mark the 0.02 and 0.98 quantiles of the d and θ distributions. The composite anomalies in SLP for the four regions delimited by the black lines are plotted as side panels and can be associated with known weather regimes: NAO+ (minima of d), NAO- (minima of θ), Atlantic Ridge (maxima of θ), Blocking (maxima of d). The black lines indicates the region where at least the 2/3 of extreme pressure anomalies have the same sign.

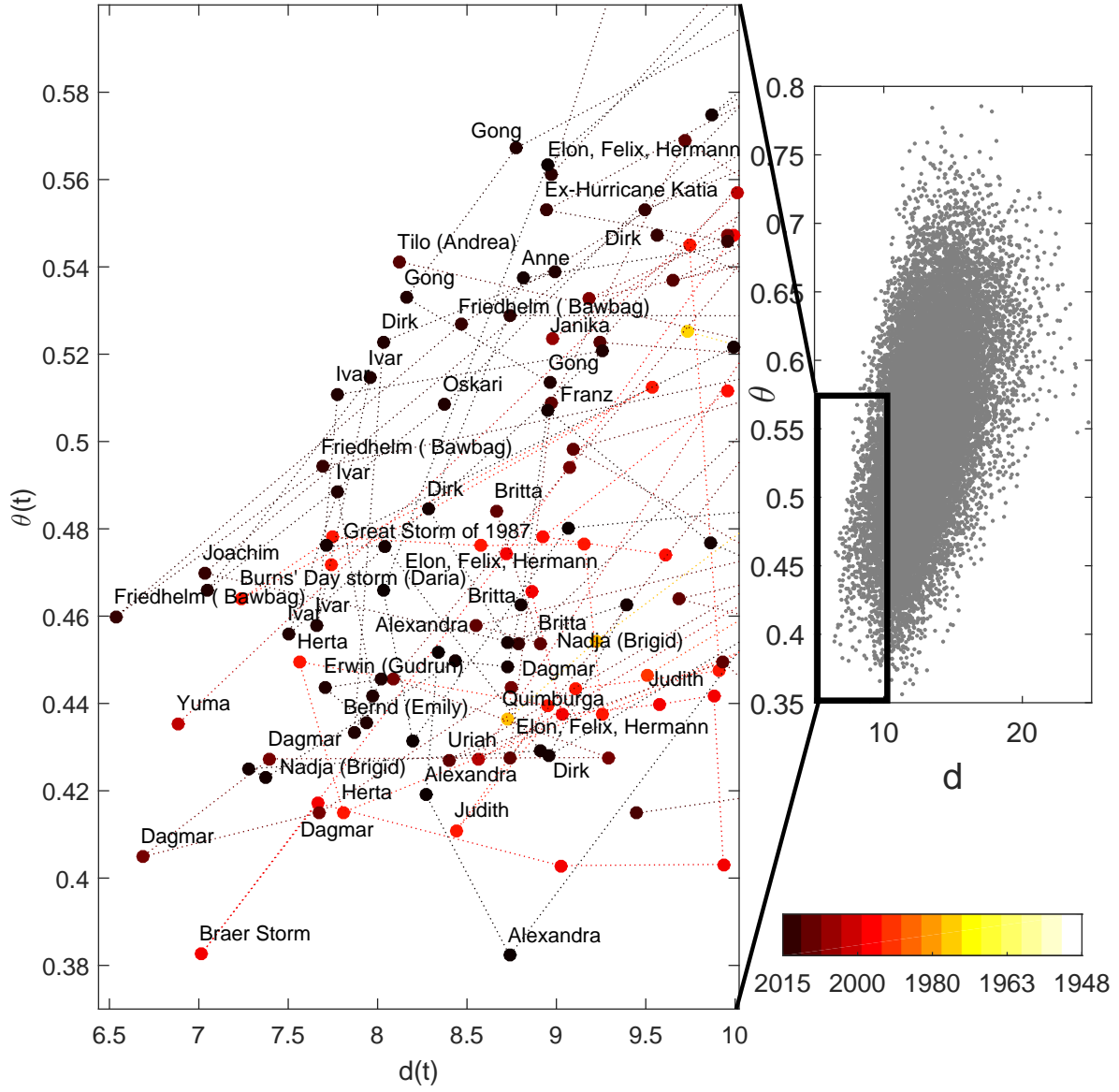


Figure 4: **Storms matching the minima of the instantaneous dimensions.** Instantaneous dimensions d (x-axis) and persistence θ (y-axis) are plotted along with names and years (colourscale). The inset shows the full distribution of d, θ values. Repeated names indicate storms which persist for several days (see supplementary storm database).

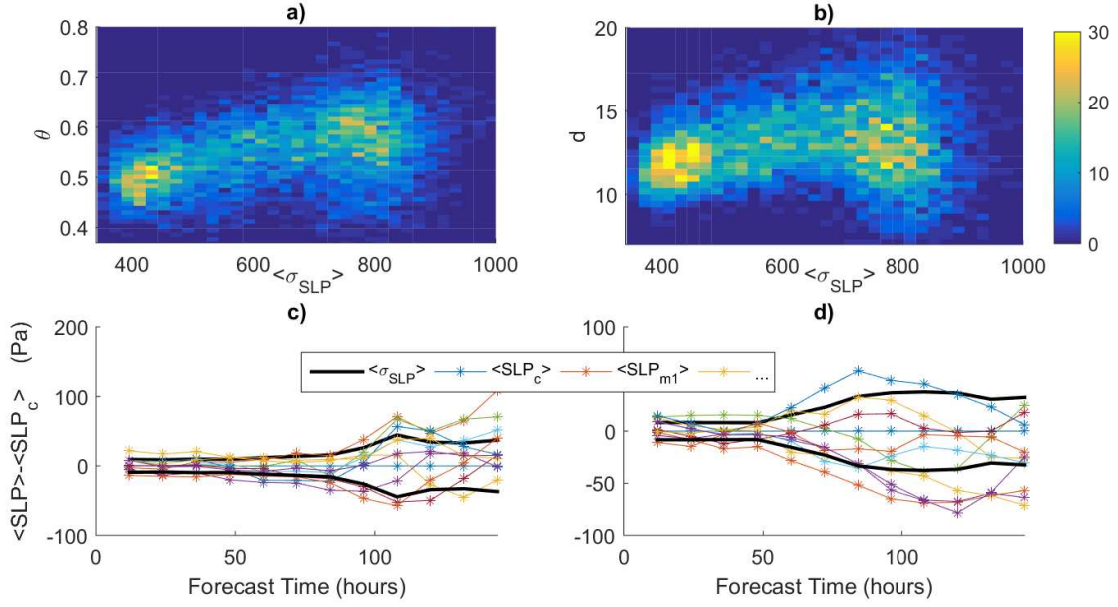


Figure 5: **Analysis of the relation between instantaneous properties and NOAA GER re-forecast.** a) and b) bivariate histograms of the ensemble spread $\langle \sigma_{SLP} \rangle$ at step +384h as a function of the stability θ (a) and the instantaneous dimension d (b) of the initialisation field. for the period 2000-2015. Colourscale indicates the number of days with the same pair of parameters. c) and d): case studies on how the Reforecast trajectories diverge from the control run $\langle SLP_c \rangle$ and their relation with ensemble spread, d and θ . c) Reforecast for the 21/01/2000 corresponding to high $d \simeq 18$ with a moderate value of $\theta = 0.56$. d) Reforecast for the 12/01/2000 corresponding to high $\theta = 0.73$ and moderate value of $d=14$.